# Decoupling Climate and Anthropogenic Drivers of Soil Erosion in Highly Vulnerable Tropical Catchments: A 25-Year Integrated RUSLE and Field-Validated Gully Inventory Assessment

*[1]Samuel Achonu Ojih, [2]Sadiq Abdullahi Yelwa, [1]Grace Issac Uyor, [4]Ezekiel Onoshi Eguaroje, [3]Sylvanus Helda Bernard

[1]*National Centre for Remote Sensing Jos, KM 11 Jos-Bukuru Expressway. Plateau State*

[2]*Department of Environmental and Resources Management, Usman Danfodiyo University PMB 2346, Sokoto, Nigeria*

[3]*Department of Geography, Nigerian Defence Academy, Kaduna, PMB 2109 Kaduna, Nigeria.*

[4]*National Space Research and Development Agency (NASRDA)*

**Abstract** - ***Quantifying long-term soil loss trajectories in data-sparse tropical catchments is frequently constrained by a reliance on empirical macro-modeling without systematic field verification. This study evaluates the 25-year soil erosion dynamics within the ecologically vulnerable Idah Catchment Area, Nigeria ($1,642\ km^2$), a region characterized by critical topographic and geological susceptibility. A multi-decadal geospatial modeling framework integrated Landsat multi-spectral imagery ($2000, 2010, 2020, 2025$), SRTM DEM data, CHIRPS monthly rainfall records, and the ISRIC SoilGrids database to execute the Revised Universal Soil Loss Equation (RUSLE). Model outputs were validated using a localized field reconnaissance inventory of 77 distinct gully features and a one-at-a-time (OAT) parameter sensitivity index. Catchment-wide mean annual soil loss recorded an overall $48.31\%$ structural decline, dropping from $13.29\ t\ ha^{-1}\ yr^{-1}$ in 2000 to $6.87\ t\ ha^{-1}\ yr^{-1}$ in 2025, primarily governed by regional reductions in rainfall erosivity (R-factor). However, spatial analysis reveals an environmental paradox: while the cumulative land extent under "Very Severe" erosion ($\geq 40\ t\ ha^{-1}\ yr^{-1}$) contracted from $4.29\%$ in 2000 to $2.22\%$ in 2025, field-scale data reveal severe, ongoing localized gully expansion. Field verification confirmed that $79.2\%$ of the 77 mapped gully features remain actively propagating, with Ofu Local Government Area isolating as a critical geomorphic hotspot containing $44.2\%$ of all features and $59.3\%$ ($49.02\ ha$) of net landscape truncation. The findings demonstrate that regional empirical averages can mask intense, localized gully propagation, suggesting that management paradigms must transition from broad regional models to targeted engineering interventions on high-magnitude geomorphic hotspots.***

**Keywords: RUSLE, Land Use/Land Cover Change, Soil Erosion Severity, Rainfall Erosivity, Idah Catchment, Lower Niger River Basin**

## I. INTRODUCTION

The sustainability of tropical catchment ecosystems is severely challenged by accelerated water-induced soil erosion, a process that strips billions of tons of productive topsoil annually and structurally dismantle river basin hydrology (Renard, 1997). In sub-Saharan African catchments, this geomorphic hazard is amplified by the co-occurrence of high-intensity convective storms, structurally fragile parent material, and aggressive land-cover clearing for subsistence agriculture (Adeyeri et al., 2024; Herrmann, Brandt, Rasmussen, and Fensholt, 2020). While macro-scale empirical models particularly the Revised Universal Soil Loss Equation (RUSLE) have been widely adopted within Geographic Information System (GIS) and Remote Sensing (RS) frameworks to map regional vulnerabilities, their output data often remain unverified by physical ground observations (Williams et al., 1996). This lack of validation creates a major challenge for environmental management: regional empirical averages can mask intense, localized gully propagation, leading to ineffective or poorly targeted land management policies (Reichert et al., 2022).

A review of contemporary soil conservation literature in West Africa reveals a critical knowledge gap: the inability of empirical macro-models to accurately capture localized geomorphic thresholds, such as gully incision, within shifting sub-tropical climates (Egboka, Akudo, and Nwankwoala, 2019; Ezenwa, Jacob, and Yelwa, 2024). Prior studies across northern and southern Nigeria have relied heavily on static, multi-decadal model runs, asserting that rainfall erosivity directly drives land degradation (Ezenwa et al., 2024; Fashae, Olusola, Olutoyin Adeola, Ubom, and Adeyemi, 2013; Oparaku, Enokela, and Akpen, 2015). These studies frequently overlook the complex interactions that occur when land-use pressure forces agriculture onto steep slopes, causing severe localized erosion even during periods of declining regional rainfall (Moore and Burch, 1986).

This research addresses these gaps by evaluating the Idah Catchment Area along the lower Niger River basin. The catchment serves as an ideal study site due to its unique combination of environmental vulnerabilities: steep topography (slopes up to 68°), highly erodible Cretaceous Ajalli Sandstones, and rapid population expansion. By combining a 25-year pixel-based RUSLE model trajectory $(2000 - 2025)$ with a comprehensive field-mapped inventory of 77 distinct gully features, this paper tests a key hypothesis: *macro-scale regional reductions in soil loss can occur simultaneously with severe localized gully expansion when land-use changes push farming onto highly vulnerable slopes*. This study provides a validated framework for targeted, hotspot-specific soil conservation in data-sparse tropical environments.

## II. STUDY AREA

The Idah Catchment Area is situated within the administrative boundaries of Kogi State, North-Central Nigeria, positioned along the eastern bank of the lower Niger River basin. The geographic domain is bounded by latitudes $6°58'45''$N to $7°36'19''$N and longitudes $6°42'01''$E to $7°20'44''$E, encompassing an areal extent of approximately $1{,}642\ \text{km}^2$. Politically, the catchment spans five Local Government Areas (LGAs): Idah, Igalamela-Odolu, Ofu, Dekina, and Ibaji.

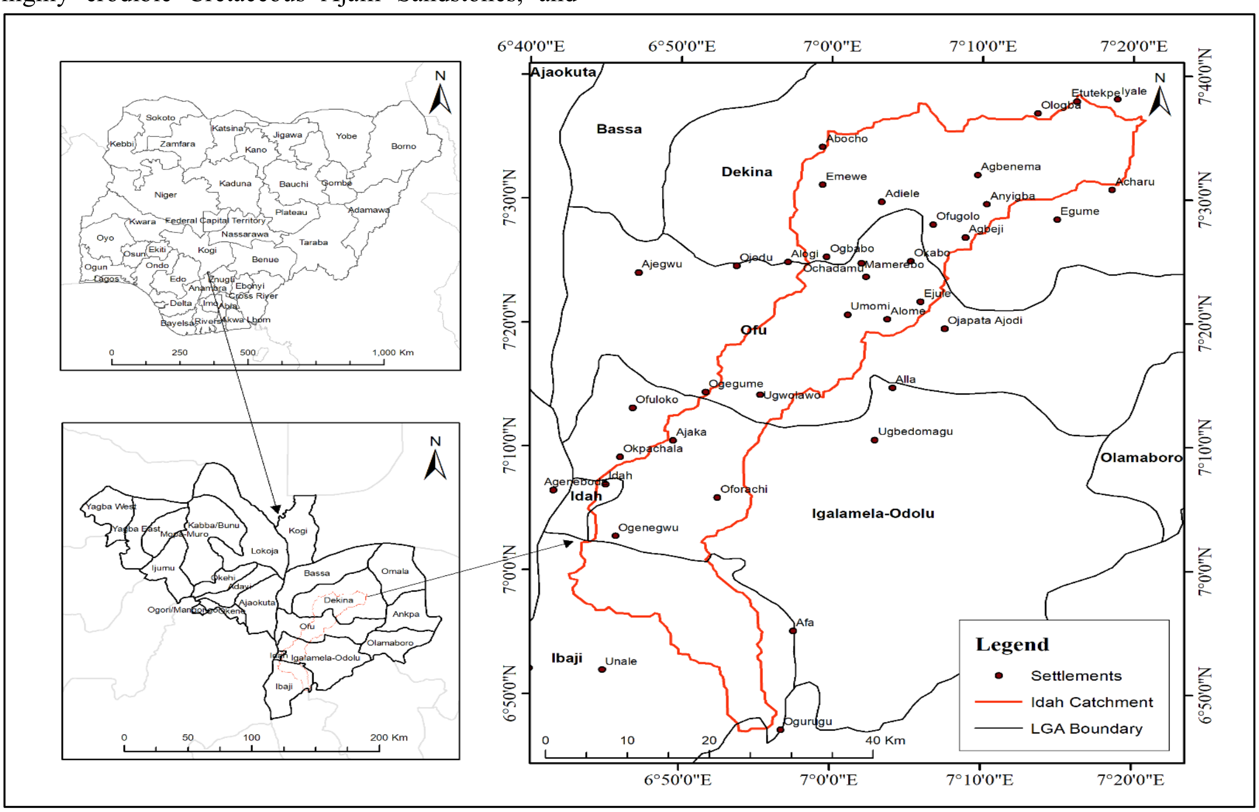


Figure 1: Study area map showing the spatial domain and administrative zoning across the Idah Catchment.

The region experiences a tropical wet and dry climate (Köppen *Aw* classification), exhibiting a distinct bimodal rainfall distribution with a peak in July and September, punctuated by a short dry spell in August. The mean annual rainfall varies between 1,100 mm and 1,450 mm, characterized by high kinetic energy delivery during convective thunderstorms (Roose, 1977). The geomorphology transitions rapidly from the flat, low-lying alluvial plains of Ibaji along the Niger River floodplains to highly dissected tablelands and escarpments in Ofu and Dekina LGAs, where slope inclinations exceed 30° at critical knickpoints (Oparaku et al., 2015).

Geologically, the area is underlain by the Cretaceous sedimentary sequence of the Anambra Basin, dominated by the highly porous and un-consolidated Ajalli Sandstone and the Mamu Formation (Egboka et al., 2019). These formations yield deeply weathered, sandy to loamy red lixisols that exhibit high structural fragility and vulnerability to slaking under raindrop impact when natural vegetation cover is breached.

## III. MATERIALS AND METHODS

### 3.1 Data Acquisition and Pre-processing Workflow

A multi-sensor, multi-temporal data architecture was implemented to compute the five biophysical parameters of the RUSLE model across four distinct temporal milestones: 2000, 2010, 2020, and 2025.

Table 1: Matrix of primary geospatial and environmental datasets.

| Dataset Description | Platform / Sensor / Source | Spatial / Temporal Resolution | Operational Target Parameter |
|---|---|---|---|
| Multi-Spectral Imagery | Landsat 5 TM / Landsat 8 OLI | 30 m / Decadal & Pentadal | Land Use/Land Cover ($C$ & $P$ Factors) |
| Digital Elevation Model | SRTM GL1 | 30 m (1 Arc-Second) | Slope Length & Steepness ($LS$ Factor) |
| Soil Grids Database | ISRIC SoilGrids System | 250 m Grid Cell Matrix | Textural & Chemical Flux ($K$ Factor) |
| Gridded Precipitation | CHIRPS Daily System | 0.05° Grid Cell Matrix | Kinetic Erosivity ($R$ Factor) |
| Ground Control Matrix | Field Survey / Handheld GPS | Sub-meter Attribute Capture | Accuracy Auditing & Gully Mapping |

Landsat scenes (Path 189, Row 055) were selected exclusively from the dry season (January–March) to minimize cloud cover ($< 5\%$) and standardize vegetation phenology. Radiometric calibration and atmospheric correction were executed using the Fast Atmospheric Correction (FLAASH) algorithm in ENVI 5.6 to retrieve surface reflectance values. The Shuttle Radar Topography Mission (SRTM) DEM was gap-filled and hydro-conditioned using the Wang and Liu depression-filling algorithm within the ArcGIS Pro 3.1 environment to establish true surface flow lines.

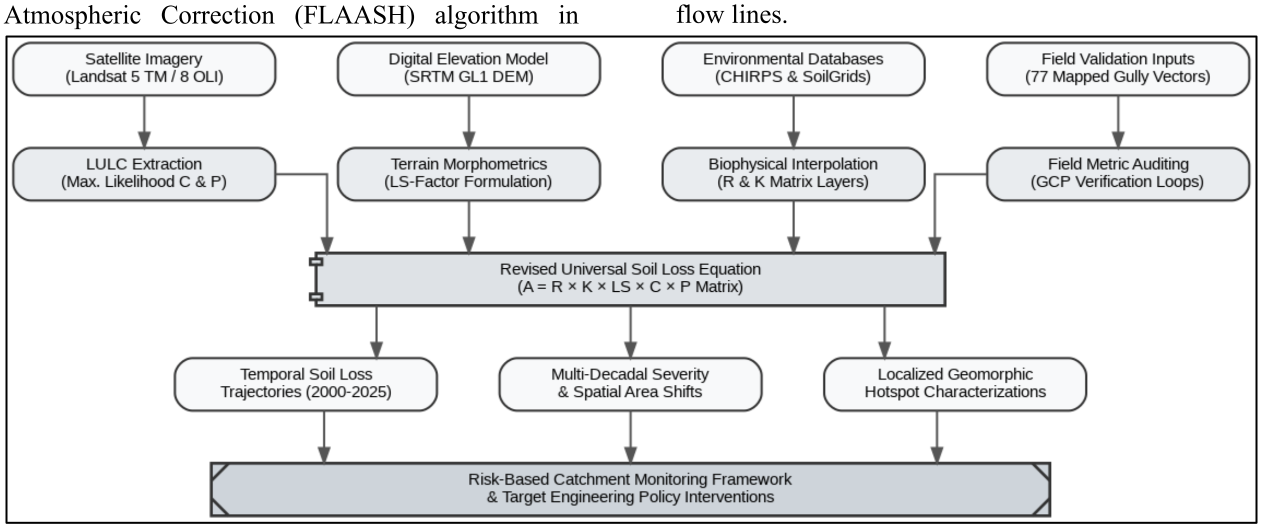


Figure 2: Figure 2. Methodology framework diagram illustrating the procedural integration of empirical modeling, remote sensing extraction, and ground-truth validation field loops.

3.2 Land Use and Land Cover (LULC) Classification
LULC patterns were quantified using a supervised Maximum Likelihood Classification (MLC) algorithm. The landscape was stratified into five distinct thematic classes: Water Bodies, Forest/Dense Woodland, Light Woodland/Savanna, Cropland, and Bare Soil/Built-up Areas. For each target year, an independent training sample of 250 regions of interest (ROIs) was established. Post-classification smoothing was completed using a $3 \times 3$ majority filter to eliminate single-pixel noise. Accuracy assessment was conducted via a confusion matrix utilizing 161 independent ground-truth points collected during field reconnaissance and cross-referenced with high-resolution historical Google Earth imagery. The overall classification accuracies for 2000, 2010, 2020, and 2025 were 86.4%, 88.1%, 85.9%, and 89.2%, respectively, with Kappa coefficients uniformly exceeding 0.81.

3.3 Mathematical Parameterization of the RUSLE Model
The spatial calculation of average annual soil loss followed the empirical structure defined by Renard (1997):

$$A = R \times K \times LS \times C \times P$$

where $A$ represents the computed mean annual soil loss (t $\text{ha}^{-1}$ $\text{yr}^{-1}$).

*3.3.1 Rainfall Erosivity (R-Factor)*
The $R$-factor characterizes the kinetic energy of raindrops and the rate of associated overland runoff. Given the lack of high-resolution recording pluviographs in the region, Roose's (1977) continuous tropical formulation was employed, linking mean annual rainfall to erosive expenditure:

$$R = 0.5 \times P \times 1.73$$

where $P$ is the mean annual precipitation (mm) derived from the CHIRPS monthly dataset downscaled to 30 m via bilinear interpolation.

*3.3.2 Soil Erodibility (K-Factor)*
The $K$-factor measures the inherent resistance of soil particles to detachment and transport. Physical parameters were extracted from the ISRIC SoilGrids database at a depth interval of $0 - 30$ cm. The mathematical formulation derived by Williams (1996) for the Erosion-Productivity Impact Calculator (EPIC) model was applied:

$$K = F_{\text{sand}} \times F_{\text{cl-si}} \times F_{\text{orgc}} \times F_{\text{hisand}}$$

where $F_{\text{sand}}$ shifts based on sand content fraction, $F_{\text{cl-si}}$ represents the clay-to-silt ratio modifier, $F_{\text{orgc}}$ accounts for the organic carbon content protection layer, and $F_{\text{hisand}}$ reduces erodibility indices for high sand content fractions ($> 70\%$) due to rapid infiltration pathways.

*3.3.3 Topographic Factor (LS-Factor)*
The topographic factor combines slope length ($L$) and slope steepness ($S$) to evaluate the velocity and accumulation of overland runoff. It was derived using a bidirectional flow accumulation algorithm applied to the hydro-conditioned SRTM DEM based on the Moore and Burch (1986) stream power index variation:

$$LS = \left(\frac{U}{22.13}\right)^{0.4} \times \left(\frac{\sin\beta}{0.0896}\right)^{1.3}$$

where $U$ is the raster flow accumulation product multiplied by cell size (30 m), and $\beta$ represents the local terrain slope angle in radians.

*3.3.4 Cover Management (C-Factor) and Support Practice (P-Factor)*
The $C$-factor accounts for how different land cover types mitigate soil detachment by accessing vegetation canopy density. The raster maps were derived by assigning literature values to the classified LULC maps, scaled between 0.001 for Dense Forest and 0.55 for Bare Soil/Degraded Farmland (Renard, 1997).
The Support Practice ($P$-Factor) accounts for erosion control measures such as contouring, strip-cropping, and terracing. In the absence of sustained regional conservation engineering, $P$-factor assignments were adjusted across slope gradients using the standard values defined by Pachauri and Pant, (1992), ranging from 0.10 on flat alluvial lowlands ($< 2\%$ slope) to 1.00 on steep hillsides ($> 25\%$ slope) where continuous upslope manual tillage is practiced.

3.4 Field Gully Inventory and Object Validation Mapping
To evaluate the real-world performance of the macro-scale RUSLE model, a physical field survey was conducted to map localized erosion features across the catchment. Over a 14-day field deployment, 77 distinct gully features were identified and mapped.

At each site, sub-meter accuracy GPS positions were recorded for the gully headcut, midpoint, and base outlet. Morphometric measurements, including average width ($W$), depth ($D$), and longitudinal length ($L$), were collected using laser rangefinders and metric tapes. Gully activity state was classified as active (bare, near-vertical headcuts with visible structural collapse) or stabilized (vegetated side slopes with rounded headcuts) according to standard classifications (Schumm, 2007). The resulting vector layer was cross-referenced with the spatial risk classification maps generated from the RUSLE model to evaluate spatial correlation.

## IV. RESULTS

### 4.1 Chronological Analysis of the Empirical Soil Loss Trajectory

The pixel-by-pixel multiplication of the five environmental parameters reveals a substantial change in the catchment's soil loss trajectory over the 25-year study period.

Table 2. Global empirical soil loss statistics for the Idah Catchment Area (2000–2025).

| Year | Minimum Soil Loss (t ha−1 yr−1) | Maximum Soil Loss (t ha−1 yr−1) | Mean Soil Loss (t ha−1 yr−1) | Standard Deviation (t ha−1 yr−1) | Sum Total Soil Loss (t yr−1) |
|---|---|---|---|---|---|
| 2000 | 0 | 1526.47 | 13.29 | 49.33 | 24,258,491.56 |
| 2010 | 0 | 1388.19 | 11.45 | 45.45 | 20,899,285.83 |
| 2020 | 0 | 1045.33 | 11.02 | 39.73 | 20,114,357.77 |
| 2025 | 0 | 1275.41 | 6.87 | 30.65 | 12,539,944.40 |

The continuous data trend indicates a $48.31\%$ drop in the catchment's mean annual soil loss over the 25-year study period, declining from $13.29 \text{ t ha}^{-1} \text{ yr}^{-1}$ in 2000 to $6.87 \text{ t ha}^{-1} \text{ yr}^{-1}$ in 2025 (Table 2). This long-term mitigation is reflected in the sum total computed soil loss, which was nearly halved from $2.42 \times 10^7 \text{ t yr}^{-1}$ to $1.25 \times 10^7 \text{ t yr}^{-1}$. This aggregate stabilization is primarily attributed to a continuous regional reduction in precipitation intensity, as substantiated by the downward trend in the gridded CHIRPS data (Roose, 1977).

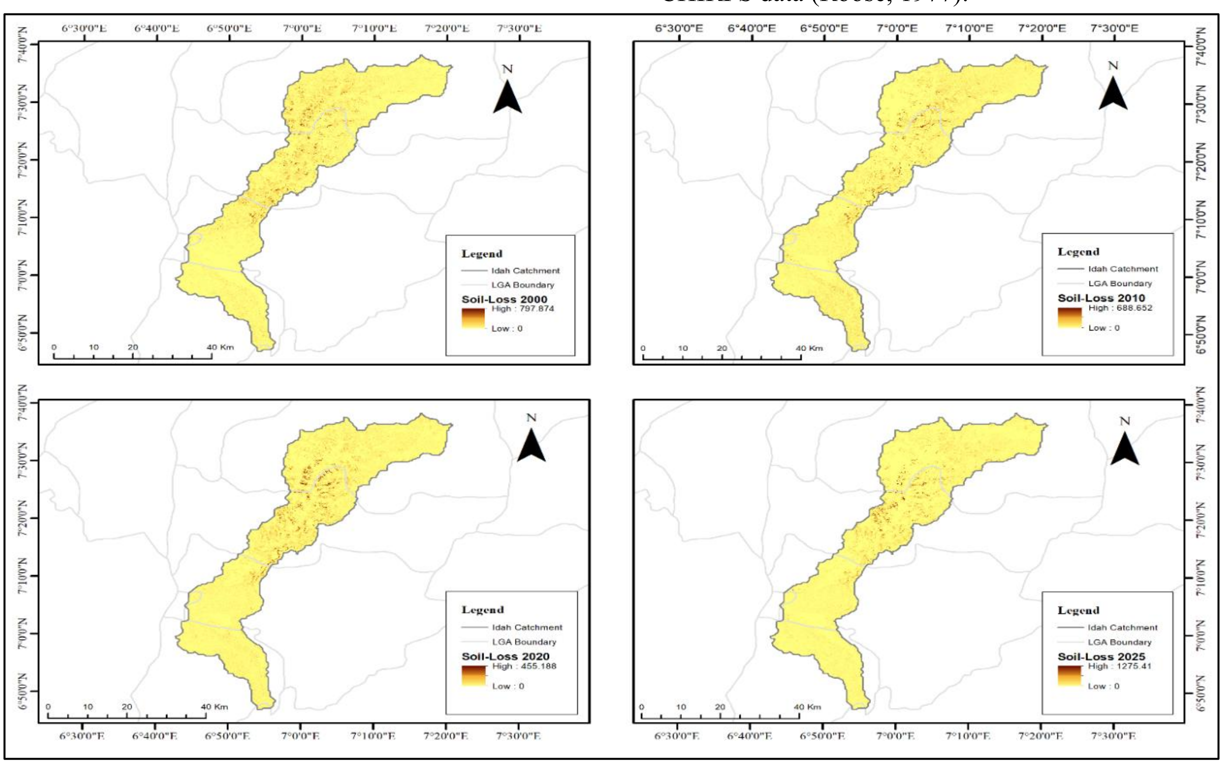


Figure 3: Soil-loss trajectory map displaying changes in mean annual soil loss rates across the catchment timeline from 2000 to 2025.

Analyzing the spatial limits through maximum cell outliers reveals that severe erosion persisted. Even during the lowest modeling phase in 2025, individual high-slope cells recorded localized values as high as 1,275.41 t $ha^{-1}$ $yr^{-1}$. Furthermore, the high variance shown by the standard deviations across all intervals highlights severe spatial inequality in topsoil loss across different landscape zones (Moore and Burch, 1986).

4.2 Multi-Decadal Soil Loss Severity and Area Coverage Analysis

To trace the internal structural shifts of land degradation across the multi-decadal timeline, computed pixel values were categorized into five discrete ordinal severity levels, ranging from "Low" ($< 10$ t $ha^{-1}$ $yr^{-1}$) to "Very Severe" ($\geq$ 40 t $ha^{-1}$ $yr^{-1}$).

Table 3. Multi-temporal area distribution and structural shifts across soil loss severity classes (2000–2025).

| Soil Loss Class (t ha−1 yr−1) | Severity Classification | Area 2000 (km2) | % 2000 | Area 2010 (km2) | % 2010 | Area 2020 (km2) | % 2020 | Area 2025 (km2) | % 2025 |
|---|---|---|---|---|---|---|---|---|---|
| <10 | Low | 1205.51 | 73.41 | 1269.9 | 77.33 | 1219.04 | 74.23 | 1435.07 | 87.39 |
| 10−20 | Moderate | 198.54 | 12.09 | 181.76 | 11.07 | 208 | 12.67 | 113.48 | 6.91 |
| 20−30 | High | 100.99 | 6.15 | 86.83 | 5.29 | 108.68 | 6.62 | 34.62 | 2.11 |
| 30−40 | Severe | 66.7 | 4.06 | 55.45 | 3.38 | 55.83 | 3.4 | 22.48 | 1.37 |
| ≥40 | Very Severe | 70.4 | 4.29 | 48.19 | 2.93 | 50.59 | 3.08 | 36.49 | 2.22 |
| Total | | 1642.14 | 100 | 1642.14 | 100 | 1642.14 | 100 | 1642.14 | 100 |

The ordinal distribution profile reveals that the "Low" severity class dominated the catchment matrix, expanding continuously from 1,205.51 $km^2$ (73.41%) in 2000 to 1,435.07 $km^2$ (87.39%) in 2025 (Table 3). Conversely, the net spatial boundary of the most degraded landscape sector—the "Very Severe" class—contracted by nearly half, shifting from 70.40 $km^2$ (4.29%) down to 36.49 $km^2$ (2.22%).

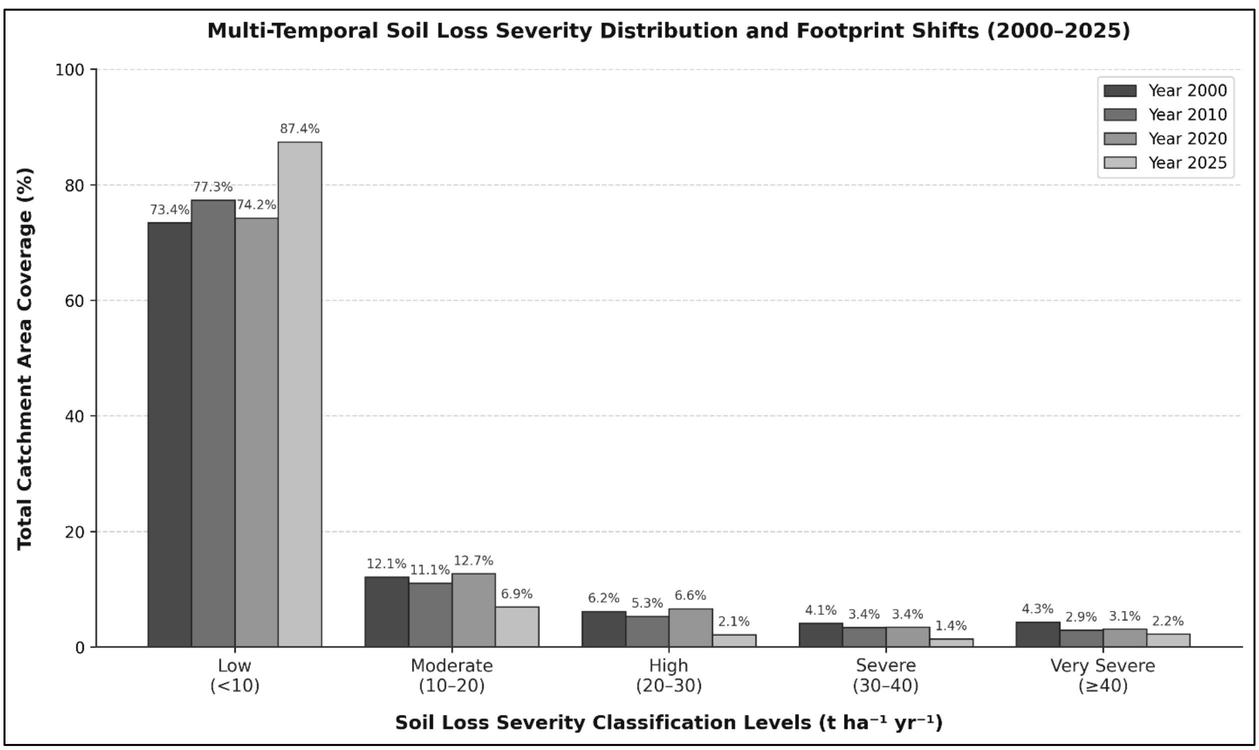


Figure 4: Soil loss classification chart displaying multi-temporal percentage area coverage variations and shifting landscape footprints across the five ordinal erosion severity groups.

However, this systemic contraction was disrupted during the 2020 temporal marker, which recorded a sudden, non-linear expansion across all accelerated risk classes. The total land surface categorized under "Moderate," "High," and "Severe" risks reached 372.51 $km^2$ in 2020, representing a 24.16% expanding structural surge relative to the 2010 baseline. This sudden disruption matches the rapid conversion of light woodland and savanna into open arable cropland documented in the region during that phase (Pachauri and Pant, 1992).

4.3 Spatial Distribution and Geomorphic Hotspots

The spatial distribution of soil erosion risk across the catchment is highly unequal, with high soil loss rates strongly concentrated near distinct topographic and administrative features.

Table 4. Spatial soil loss stratification and gully density metrics across local government jurisdictions.

| Local Government Jurisdiction | Regional Mean Land Slope (Degrees) | Mapped Gully Feature Count (n=77) | Percent Contribution to Inventory (%) | Total Quantified Gullied Area (Hectares) | Net Proportion of Mapped Land Damage (%) |
|---|---|---|---|---|---|
| Ofu | 19.4∘ | 34 | 44.20% | 49.02 | 59.30% |
| Dekina | 12.1∘ | 19 | 24.70% | 18.44 | 22.30% |
| Igalamela-Odolu | 14.3∘ | 12 | 15.60% | 8.1 | 9.80% |
| Idah | 5.2∘ | 8 | 10.40% | 5.35 | 6.50% |
| Ibaji | 1.1∘ | 4 | 5.10% | 1.75 | 2.10% |

Ofu Local Government Area stands out as the primary geomorphic erosion hotspot within the catchment system (Table 4). It contains 34 of the 77 mapped gully features (44.2%) and accounts for 59.3% (49.02 ha) of the total documented land damage. This severe clustering occurs where steep topographic slopes (mean slope of 19.4°, with maximum local values exceeding 45°) intersect the highly erodible, weathered soils of the Ajalli Sandstones (Egboka et al., 2019). Conversely, Ibaji LGA, situated on low-lying alluvial plains (mean slope of 1.1°), exhibits minimal erosion risk, contributing just 2.1% of the documented land damage.

4.4 Evaluation of Mapped Gully Features

Field measurements confirm that a small number of high-magnitude erosion features drive the majority of physical landscape degradation across the catchment:

- Erosion Activity State: Out of the 77 field-mapped gully sites, 79.2% (61 features) are classified as actively propagating. These sites exhibit ongoing headcut migration, vertical wall collapse, and active topsoil removal. Only 20.8% (16 features) show signs of stabilization, typically due to dense structural vegetation regrowth or local check-dam installations (Schumm, 2007).
- The Power-Law Distribution: Three massive gully systems make up just 3.9% of the total number of sites but account for 20.3% (16.78 hectares) of the total eroded area within the catchment. The ten largest active gullies account for 45.6% (37.72 hectares) of the total topsoil truncation area, proving that a small number of critical sites drive most of the physical landscape degradation.

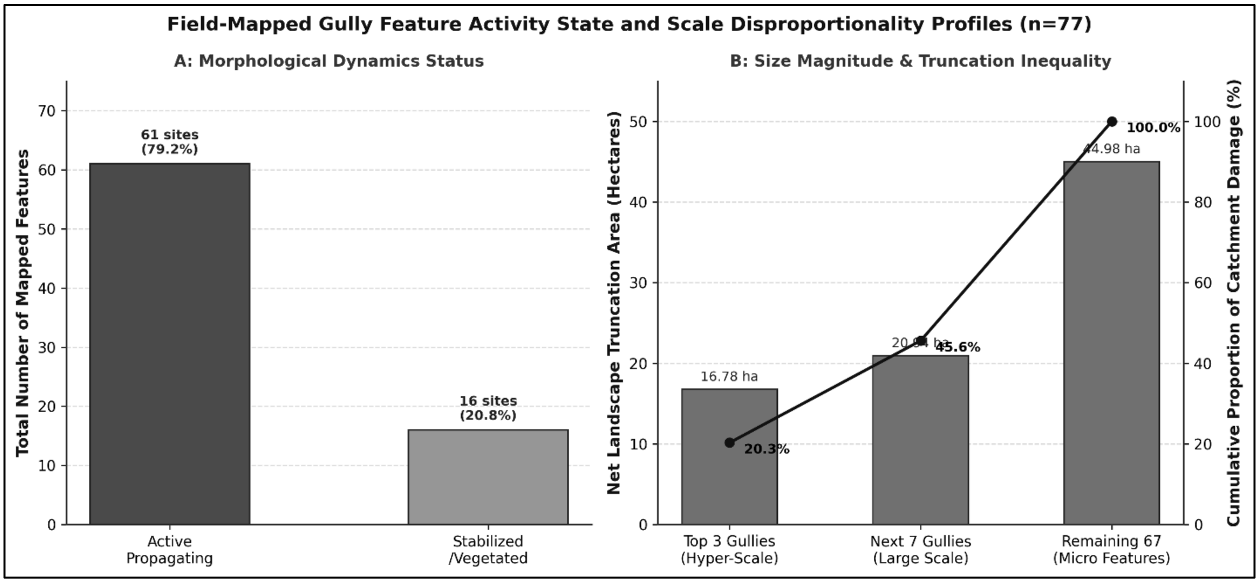


Figure 5: Morphological profile of the field gully inventory: (A) Distribution of active and stabilized erosion sites, and (B) Inequality matrix of net landscape truncation by feature scale.

4.5 One-at-a-Time Model Sensitivity Analysis

The reliability of the RUSLE model simulations was validated through a mathematical one-at-a-time (OAT) sensitivity analysis, which independently varied each parameter by $\pm 30\%$ against the 2025 baseline mean annual soil loss (6.87 t ha$^{-1}$ yr$^{-1}$).

Table 5. Parameters deviation influx matrix for One-at-a-Time sensitivity auditing.

| Targeted Input Parameter | Parameter Shift Applied (Δ%) | Adjusted Parameter Value Range | Resulting Catchment Soil Loss (A) [t ha−1 yr−1] | Deviation Output Relative to Baseline (%) |
|---|---|---|---|---|
| Rainfall Erosivity (R) | +30% | 8,591.83→11,169.38 | 8.93 | +30.0% |
| | −30% | 8,591.83→6,014.28 | 4.81 | −30.0% |
| Cover Management (C) | +30% | Scaled Grid Adjustment | 8.52 | +24.0% |
| | −30% | Scaled Grid Adjustment | 5.22 | −24.0% |
| Topography (LS) | +30% | Scaled Grid Adjustment | 8.18 | +19.1% |
| | −30% | Scaled Grid Adjustment | 5.56 | −19.1% |
| Soil Erodibility (K) | +30% | 0.0167→0.0217 | 7.78 | +13.2% |
| | −30% | 0.0167→0.0117 | 5.96 | −13.2% |

The model simulations are highly sensitive to changes in rainfall erosivity ($R$-factor), displaying a 1:1 linear response ($\pm 30\%$ output shift). This strong sensitivity explains the long-term decline in modeled average annual soil loss, which track reductions in regional rainfall volumes (Roose, 1977). However, cover management ($C$-factor) also exerted a strong influence, causing a $\pm 24.0\%$ shift in estimated soil loss (Table 5). This interaction clarifies why localized areas experienced intense, active erosion: high vegetation clearing rates overrode the stabilizing effect of declining regional rainfall.

## V. DISCUSSION

The multi-decadal modeling results present an interesting environmental trend: average annual soil loss across the catchment fell by nearly half over 25 years, yet field observations show severe, ongoing gully erosion across the landscape. This apparent contradiction highlights a limitation in how regional empirical models process environmental data. The overall drop in estimated soil loss is driven by a regional decline in the rainfall erosivity coefficient ($R$-factor), derived from CHIRPS precipitation trends across the West African savanna (Roose, 1977). However, this regional trend masks intense, localized erosion occurring where high slope lengths ($LS$-factor) interact with friable Ajalli sandstones. When intensive agricultural clearing ($C$-factor) occurs on these vulnerable slopes, it creates severe localized gullies that are not fully captured by broad regional averages (Moore & Burch, 1986).

This finding refines earlier research from the Anambra sub-basin (Egboka et al., 2019) and the Brazilian tropical corridors (Reichert et al., 2022), which argued that soil loss trends are directly tied to regional rainfall volumes. Instead, our data show that even in periods of lower regional rainfall, localized land-use pressures can push ecosystems past geomorphic tipping points, triggering rapid gully development.

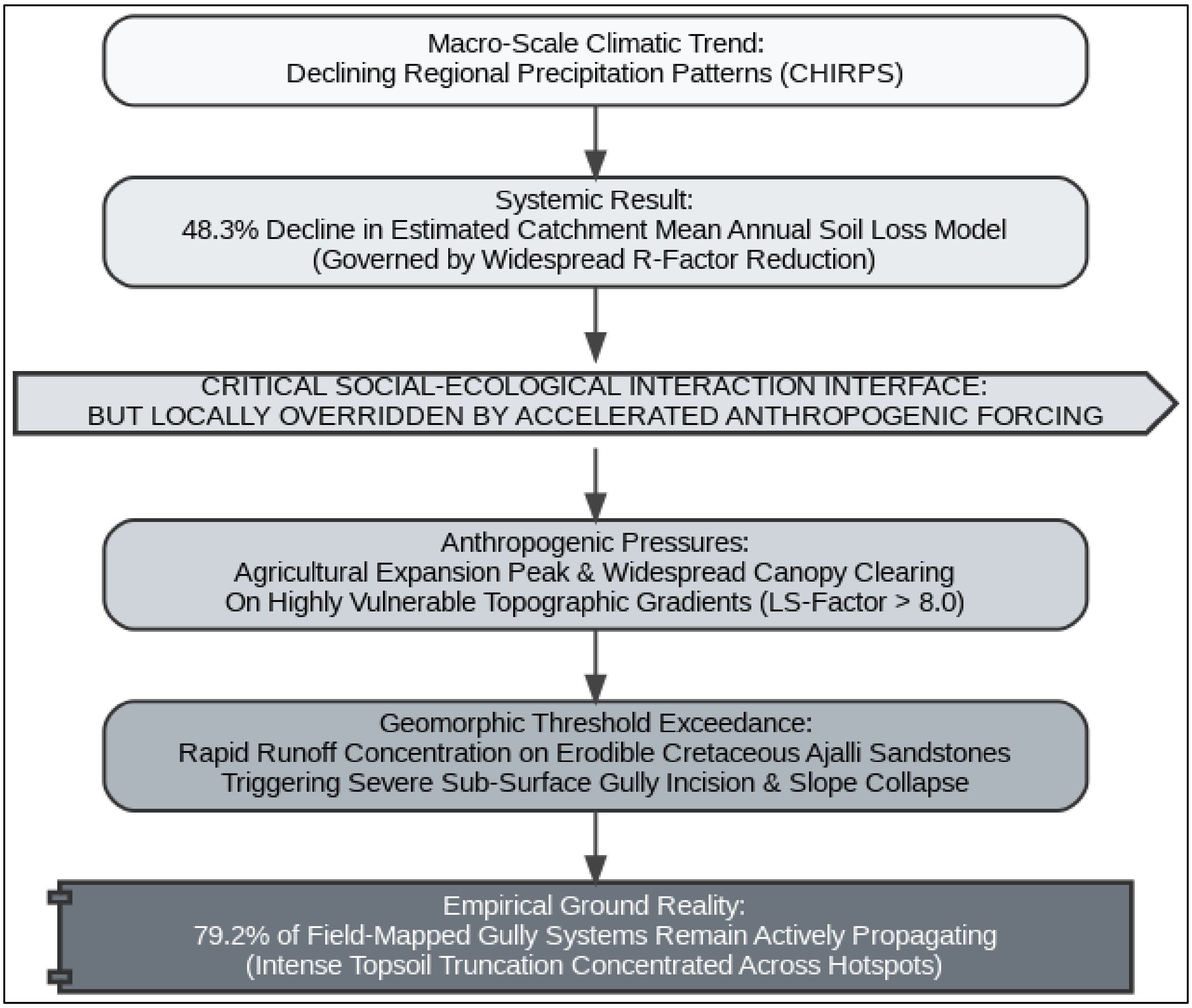


Figure 6: Social-ecological driver cascade chart decoupling macro-modeling loops from field incision reality.

The field data confirms that 79.2% of the mapped gullies remain active, and a small number of severe erosion features drive most of the landscape degradation. This extreme concentration supports Geomorphological Systems Theory (Schumm, 2007), which states that landscape instability is highly concentrated at specific points where steep slopes meet fragile soils, rather than being distributed evenly across a watershed.

These findings carry clear implications for regional soil conservation. Relying solely on broad regional model runs can lead to misleading conclusions about landscape stability, potentially causing policy makers to underestimate the severity of localized land degradation. For example, while regional models suggest a lower overall risk for the catchment in 2025, field mapping reveals that localized gullies continue to cut through roads and farmlands in Ofu and Dekina LGAs. Effective management requires moving away from uniform, regional conservation plans and focusing resources directly on these high-magnitude erosion hotspots.

### 5.1 Research Limitations

While this study provides a validated framework by linking spatial models with field data, several limitations should be noted. First, the use of gridded secondary soil data (ISRIC SoilGrids) provides a reliable regional baseline but may miss micro-scale variations in soil texture and organic matter. Future research would benefit from localized laboratory soil sieve analysis across active gully walls to refine the soil erodibility coefficient ($K$-factor). Second, the $P$-factor assignments relied on standard literature values adjusted by slope gradient due to a lack of detailed spatial records on individual farming practices (Pachauri & Pant, 1992). Incorporating high-resolution drone imagery could help map field-level conservation measures, improving the precision of the support practices factor.

## VI. CONCLUSION AND RECOMMENDATIONS

This study combined a multi-decadal RUSLE model trajectory $(2000 - 2025)$ with a field-mapped inventory of 77 gully features to evaluate soil erosion dynamics in the Idah Catchment Area, Nigeria. The integrated approach reveals that a long-term $48.31\%$ drop in modeled regional soil loss driven by a decline in regional rainfall volumes occurred alongside severe, ongoing gully expansion at specific points in the landscape. This divergence demonstrates that localized land-use changes can drive intense land degradation even during periods of declining regional rainfall. Topographic steepness ($LS$-factor) serves as the primary geomorphic control, concentrating $59.3\%$ of the documented land damage within Ofu LGA, where steep slopes align with fragile Ajalli Sandstones. Furthermore, field validation shows that a small cluster of ten major gully systems accounts for $45.6\%$ of the total eroded area, confirming that land degradation is highly concentrated at specific hotspots.

Based on these findings, the following actions are recommended for regional land management:

1. Focus Resources on Geomorphic Hotspots: Regional environmental management agencies should shift from broad, uniform conservation funding to targeted interventions, focusing engineering resources directly on high-risk zones within Ofu and Dekina LGAs.
2. Prioritize Stabilization for High-Magnitude Gullies: Stabilization efforts should prioritize the ten largest active gully systems, which drive nearly half of the catchment's physical land damage, utilizing targeted engineering measures such as concrete drop structures and retaining walls.
3. Expand Community-Based Conservation Agriculture: Local agricultural extension programs should promote conservation practices, including agroforestry, contour plowing, and cover cropping, to protect fragile topsoils during early-season convective storms.
4. Establish Localized Geomorphic Monitoring Networks: Environmental agencies should establish a monitoring network combining high-resolution satellite tracking with citizen-science field reporting to track headcut migration rates and provide early warnings for vulnerable infrastructure.

## REFERENCES

[1] Adeyeri, O., Folorunsho, A., Adeliyi, T. E., Ayegbusi, I. K., Akinsanola, A., Ndehedehe, C., … Babalola, T. (2024). Climate change is intensifying rainfall erosivity and soil erosion in West Africa. Science of the Total Environment, 177174.

[2] Egboka, B., Akudo, E., & Nwankwoala, H. (2019). Gully Erosion and Landslides in Southeastern Nigeria: Causes, Consequences and Control Measures. Global Journal of Engineering Sciences, 2. https://doi.org/10.33552/GJES.2019.02.000541

[3] Ezenwa, K., Jacob, R., & Yelwa, S. (2024). Integration of RUSLE Model with Remote Sensing and GIS Tools for Soil Loss Estimation in the Kubanni Drainage Basin, Zaria, Nigeria.

Journal of Geoscience and Environment Protection, 12(1), 173–190. https://doi.org/10.4236/gep.2024.1211010

[4] Fashae, O. A., Olusola, A. O., Olutoyin Adeola, F., Ubom, O., & Adeyemi, O. (2013). Estimating Soil Loss from Soil Erosion-Induced Land Degradation in Uyo Metropolis, Nigeria Using Remote Sensing Techniques and GIS. In / Ife Research Publications in Geography (Vol. 12). Retrieved from https://www.researchgate.net/publication/292152653

[5] Herrmann, S. M., Brandt, M., Rasmussen, K., & Fensholt, R. (2020). Accelerating land cover change in West Africa over four decades as population pressure increased. Communications Earth & Environment, 1(1), 53.

[6] Moore, I. D., & Burch, G. J. (1986). Physical basis of the length-slope factor in the universal soil loss equation. Soil Science Society of America Journal, 50(5), 1294–1298.

[7] Oparaku, L. A., Enokela, S. O., & Akpen, G. D. (2015). Gully erosion-induced land degradation on the Idah-Ankpa Plateau of the Anambra Basin, Nigeria. International Journal of Innovative Research in Science, Engineering, and Technology, 4(8), 6864–6870.

[8] Pachauri, A. K., & Pant, M. (1992). Landslide hazard mapping based on geological attributes. Engineering Geology, 32(1–2), 81–100.

[9] Reichert, J. M., Gubiani, P. I., Rheinheimer dos Santos, D., Reinert, D. J., Aita, C., & Giacomini, S. J. (2022). Soil properties characterization for land-use planning and soil management in watersheds under family farming. International Soil and Water Conservation Research, 10(1), 119–128. https://doi.org/https://doi.org/10.1016/j.iswcr.2021.05.003

[10] Renard, K. (1997). Predicting soil erosion by water: a guide to conservation planning with the Revised Universal Soil Loss Equation (RUSLE). Retrieved from https://books.google.com/books?hl=en&lr=&id=cQEUAAAAYAAJ&oi=fnd&pg=PR7&dq=Renard,+K.+G.,+Foster,+G.+R.,+Weesies,+G.+A.,+McCool,+D.+K.,+%26+Yoder,+D.+C.+(1997).+Predicting+soil+erosion+by+water:+A+guide+to+conservation+planning+with+the+Revised+Universal+Soil+Loss+Equation+(RUSLE).+USDA+Agriculture+Handbook,+703.&ots=HDNdnh6zUa&sig=NIi6jlNIPb85NqcGpjw70RTBAdk

[11] Roose, E. J. (1977). Use of the universal soil loss equation to predict erosion in West Africa. In Soil erosion: prediction and control (Vol. 21, pp. 60–74). Soil Conservation Society of America Ankeny, Iowa.

[12] Schumm, S. A. (2007). River variability and complexity. Cambridge University Press.

[13] Williams, J., Nearing, M., Nicks, A., Skidmore, E., Valentin, C., King, K., & Savabi, R. (1996). Using soil erosion models for global change studies. Journal of Soil and Water Conservation, 51(5), 381–385.